

Self-starting harmonic comb emission in THz quantum cascade lasers

Journal Article**Author(s):**

Forrer, Andres ; Wang, Yongrui; Beck, Mattias ; Belyanin, Alexey; Faist, Jérôme ; Scalari, Giacomo 

Publication date:

2021-03-29

Permanent link:

<https://doi.org/10.3929/ethz-b-000478146>

Rights / license:

[Creative Commons Attribution 4.0 International](#)

Originally published in:

Applied Physics Letters 118(13), <https://doi.org/10.1063/5.0041339>

Funding acknowledgement:

165639 - Monolithic, self referenced quantum cascade laser frequency comb (SNF)

Self-starting harmonic comb emission in THz quantum cascade lasers

Cite as: Appl. Phys. Lett. **118**, 131112 (2021); doi: [10.1063/5.0041339](https://doi.org/10.1063/5.0041339)

Submitted: 22 December 2020 · Accepted: 13 March 2021 ·

Published Online: 31 March 2021









View Online



Export Citation



CrossMark

Andres Forrer,^{1,a)}  Yongrui Wang,²  Mattias Beck,¹  Alexey Belyanin,²  Jérôme Faist,¹ 
and Giacomo Scalari^{1,a)} 

AFFILIATIONS

¹Institute for Quantum Electronics, Department of Physics, ETH Zürich, 8093 Zürich, Switzerland

²Department of Physics and Astronomy, Texas A&M University, College Station, Texas 77843, USA

^{a)}Authors to whom correspondence should be addressed: aforrer@phys.ethz.ch and scalari@phys.ethz.ch

ABSTRACT

Harmonic comb states have proven to be ubiquitous in mid-IR quantum cascade lasers. We report here on robust, pure, self-starting harmonic mode locking in Copper-based double-metal THz quantum cascade lasers. Different harmonic orders can be excited in the same laser cavity depending on the pumping condition, and stable harmonic combs spanning more than 600 GHz at 80 K are reported. Such devices can be RF injected, and the free running coherence is assessed by means of a self-mixing technique performed at 50 GHz. A theoretical model based on Maxwell-Bloch equations including an asymmetry in the gain profile is used to interpret the data.

© 2021 Author(s). All article content, except where otherwise noted, is licensed under a Creative Commons Attribution (CC BY) license (<http://creativecommons.org/licenses/by/4.0/>). <https://doi.org/10.1063/5.0041339>

Quantum Cascade Lasers (QCLs)^{1,2} are compact and powerful semiconductor frequency comb sources in the mid-IR³ and THz.^{4–6} They exhibit frequency modulated (FM) output, with a linear chirp over the round trip time measured for mid-IR QCLs.⁷ Their FM output properties, stabilization, and control were investigated in mid-IR^{7,8} and partially in the THz region.^{4,9–11} Finally, harmonic frequency combs operating on multiples of the fundamental round trip frequency have been reported and investigated in mid-IR QCLs^{12–14} as well as in actively mode-locked THz QCLs.¹⁵ Harmonic combs emitted by mid-IR QCLs were observed only after careful control of the optical feedback.^{12,13,16} Controlled generation of specific harmonic comb states can be achieved by optical seeding¹⁷ or by defect-engineered mid-IR QC ring lasers.¹⁸

In this Letter, we present results on robust, self-starting harmonic frequency combs in double-metal Cu–Cu THz QCLs up to temperatures of 80 K. First, we discuss different THz QCLs, which show at multiple bias points self-starting and pure harmonic comb states and report on their experimentally observed differences with respect to mid-IR QCL harmonic combs. Successively, the coherence of the spectral modes is examined via a self-mixing technique on the free running electrically detected beatnote. We also demonstrate RF injection locking of the harmonic state to an RF synthesizer. The observed harmonic comb state with an asymmetry in the spectral emission is theoretically discussed using a Maxwell-Bloch approach including two lower lasing states.

The investigated THz quantum cascade active region is a homogeneous four quantum well design based on highly diagonal transition. The upper level has two transitions to two lower levels with dipole moments of $z_{ul_1} \sim 3.0$ nm and $z_{ul_2} \sim 2.1$ nm calculated with a Schrodinger-Poisson solver at 30 K. The band structure is shown in Fig. S1 of the [supplementary material](#). These two transitions lead to an asymmetric gain profile, which significantly changes the theoretical predictions compared to a symmetric gain profile and is discussed in the theoretical part and in detail in the [supplementary material](#). The asymmetry and the roughly one order of magnitude longer gain recovery time in THz active regions^{19–21} are the main parameters different to mid-IR QCLs. The active region itself was previously studied in the fundamental frequency comb regime including injection locking in Refs. 22 and 23. The active region is embedded in either double metal gold–gold (Au–Au)²² or low loss copper–copper (Cu–Cu)²³ waveguides featuring lossy setbacks in the top cladding²⁴ for transverse mode control. As was mentioned in Refs. 22 and 23, the devices show spectral indications of self-starting harmonic comb states. In this case of Au–Au waveguides, lasing started in a single mode regime and evolves into the harmonic state, finally breaking into the fundamental/dense comb state. This mechanism mainly follows the observations on mid-IR QCLs.^{12–14} In the case of the Cu–Cu waveguide studied in this work, we observe a different behavior: the harmonic comb does not arise gradually from a single mode but emerges spontaneously

alternating with the fundamental comb or high-phase noise states. The harmonic comb state is observed at different bias points, even much higher than the laser threshold. An example of a 4.00 mm long and 64 μm wide device exhibiting the self-starting harmonic comb state from a dense state is presented in Fig. 1(a) for currents from 520 mA to 555 mA and from 780 mA to 814 mA, operating at 80 K and a lasing threshold of 390 mA. The presented spectra show the absolute values from the real part of the phase-corrected^{25,26} complex Fourier Transform from the zero-padded and with the Blackman–Harris window apodized interferogram. The absolute value was taken due to the esthetic reason in the log-scaled plots. The symmetry of the interferogram (IFG) envelope arising from equally spaced modes and its interpretation in terms of coherence and purity of the comb state are further discussed below and in Fig. 2. In Fig. 1(b), we present the intensity spectrum of a fundamental comb at a bias current of 755 mA. The electrical beatnote at 9.91 GHz is detected over a bias-tee using a 67 GHz spectrum analyzer (SA, Rohde&Schwarz, FSW67), and the RF spectrum is shown in Fig. 1(c). The observed linewidth is in the sub-kHz range. The harmonics of the fundamental beatnote and the beating of wider spaced modes are visible as well. We observe up to the sixth harmonic (59.46 GHz) of the fundamental, indicating coherence at least up to the sixth mode. The observed rise of the noise floor at 50 GHz is an intrinsic feature of the SA (dashed area). The inset shows the fundamental beatnote. Fig. 1(d), measured on the same device, shows the harmonic comb state skipping four modes at a driving current of 800 mA. In addition to the observed THz harmonic spectrum, the intra-cavity mixing of the lasing modes spaced by 5 roundtrips leads to a current modulation on the bias line, which is as

well detected over the bias tee. The single beatnote at 49.346 GHz is shown in Fig. 1(e) corresponding to the expected 5th harmonic of the cavity repetition rate ($49.346/5 \text{ GHz} = 9.8692 \text{ GHz}$). We would like to highlight here that no other beating across the RF spectrum is observed except the one of the harmonic beatnote, indicating the purity of the harmonic state. This was verified by investigating the RF spectra at the subharmonic frequencies with a lower resolution bandwidth (RBW) and a lower frequency span (not shown). The inset of Fig. 1(e) shows the single beatnote with a linewidth of $\sim 850 \text{ Hz}$ and an S/N ratio of $\sim 45 \text{ dB}$ recorded with a RBW of 300 Hz.

Compared to their Au–Au waveguide counterparts, the Cu–Cu waveguide features lower losses (4.4 cm^{-1} and 5.7 cm^{-1} at 3 THz for a lattice temperature of 150 K, 2D Comsol[®] 5.6, mirror losses and inter-subband absorption excluded), which lead to a wider dynamic range, higher maximum pumping with respect to threshold, and increased intracavity fields (roughly 0.2 kV/cm at peak). Therefore, the nonlinear effects related to four-wave mixing of laser modes become more important.

Multiple of these observed harmonic states appear for different cavity lengths and widths as well as different temperatures. Figure 2(a) shows a series of IFGs with the corresponding spectra in Fig. 2(b) for multiple devices. Specific lengths, widths, temperatures, and pumping levels and fundamental mode skipings are shown in Fig. 2(b). The center of the envelope of the modes, in contrast to mid-IR cases, is found to be in-between two modes. This asymmetry in the envelope marks a difference with respect to what was observed in mid-IR QCLs where central, more intense mode and symmetric, less intense harmonic modes are frequently observed.¹³

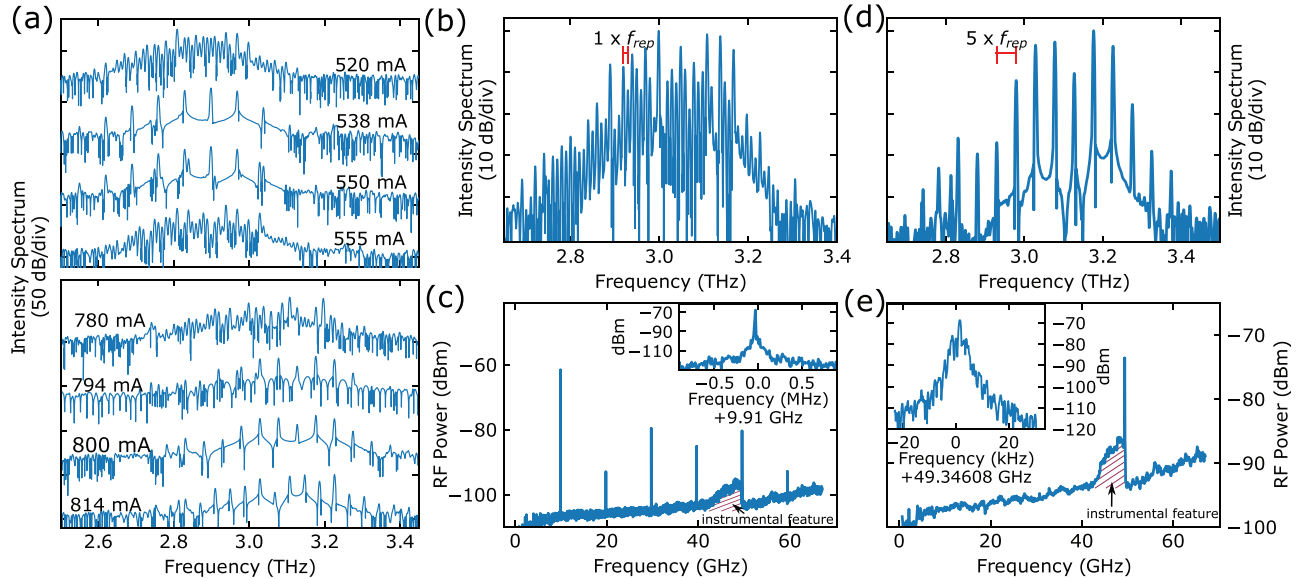


FIG. 1. Harmonic comb state in a 4 mm long and 64 μm wide double-metal Cu–Cu THz QCL at 80 K. (a) Transition from a dense state to a harmonic comb state and back for bias current from 520 mA to 555 mA and from a dense state to a harmonic state from 780 mA to 814 mA close to roll-over. Lasing threshold is at 390 mA. (b) Intensity spectrum with phase-correction, apodization, and zero-padding applied of a fundamental comb state at a bias current of 755 mA. (c) Electrically detected RF spectrum on the bias corresponding to the fundamental comb state with a narrow beatnote at 9.91 GHz and its harmonics, recorded with the 500 kHz RBW. The increasing noise floor and the transition at 50 GHz are instrumental features of the SA used. The inset shows a zoom on the fundamental BN. (d) Intensity spectrum of a harmonic comb state with phase-correction, apodization, and zero-padding applied at a bias current of 800 mA. The modes are spaced by $5 \times \text{FSR}$ of the cavity. (e) Electrically detected single beatnote at 49.346 GHz on the laser bias, recorded with the 3 MHz RBW. The absence of other beating signals indicates the purity of the harmonic state. Inset: Zoom on the harmonic beatnote with an RBW of 300 Hz presenting a linewidth of 850 Hz with optical feedback from the FTIR.

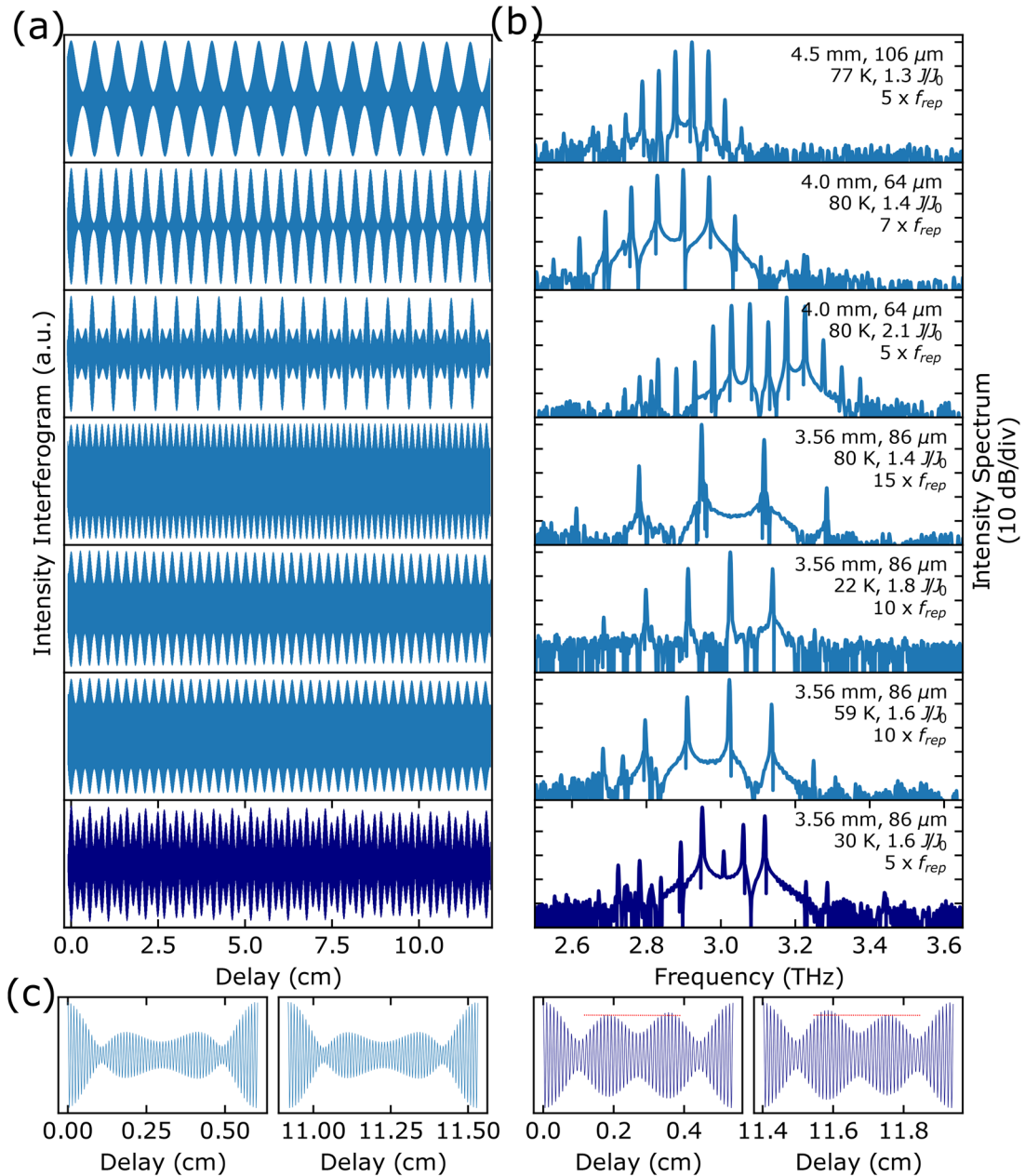


FIG. 2. (a) Shows a series of IFGs of harmonic states (light blue) and a harmonic-like state (dark-blue). (b) presents the corresponding spectra that all show similarities to harmonic comb states. (c) compares the symmetry argument, which is a required property of the harmonic comb (as well for fundamental combs), from the harmonic comb state (light blue) and the harmonic-like state (dark blue), where in the latter, the symmetry is not preserved.

As mentioned above, the coherence and purity of any comb or harmonic state can be verified to a certain degree by comparing the symmetry and periodicity of the measured IFG envelope. The equidistant spacing of the modes in a fundamental or harmonic comb leads to a periodicity of the beating signals observed in the IFG. This means that for a perfect interferometer, all modes are in-phase for delays corresponding to a multiple of the mode spacing ($dx = c/f_{rep}$) and the

measured IFG should identically repeat itself, up to a slow sinusoidal modulation with the virtual frequency f_{ceo} of the comb. For non-equidistant modes, the retardation for being in-phase is different for different mode pairs. Therefore, mode pair beatings are getting out-of-phase for increasing delay. By numerically generating IFGs similar to our case but with non-equidistant spacing, we find that a linear decrease of ~ 20 MHz in the mode spacing leads to a visible

asymmetry (also see the [supplementary material](#), Sec. VI). A roughly linear decrease in the mode spacing is expected for multi-mode operation due to the GaAs dispersed cavity modes. This 20 MHz linear decrease in the mode spacing and 280 MHz difference between the lowest and highest frequency modes of the harmonic comb are smaller than the nominal Fourier Transform resolution of 2.5 GHz of our FTIR and is clearly accessible. In the case of the comb in [Fig. 1\(b\)](#) with more modes, this symmetry argument is even valid down to the MHz level (see the [supplementary material](#)). The symmetry argument is, therefore, a powerful and readily accessible tool for verification of pure combs at the MHz level using a simple FTIR interferogram. We would like to highlight here that the same conclusion could, in principle, be made in the frequency domain as well as by using the properties of a frequency comb. But the extraction of this information in the frequency domain is not straightforward, mathematically more evolved, and, therefore, less clearly accessible than in the space domain. The IFGs in [Fig. 2\(a\)](#) exhibit such a symmetry and a periodicity except the last one. It is important to notice that the envelope is slowly decreasing due to diffraction losses and beam divergence of any real FTIR measurement and its alignment, but the symmetry within each period is conserved. The last IFG and spectrum in the dark blue show an example of a harmonic-like state that is not pure. This is shown in [Fig. 2\(c\)](#) where a zoomed version of the third IFG from top of the harmonic state (light blue) and the IFG of the harmonic-like state (dark blue) around the zero path delay (ZPD) and close to the maximum travel range of the FTIR is presented. The symmetry is preserved for the harmonic comb, whereas for the harmonic-like state, a clear asymmetry is observed. This IFG symmetry argument helps to identify non-pure comb states even in the presence of a single visible electrical beatnote or strong injection. Of course the symmetry in the IFG is a required property for a comb (fundamental or harmonic) and can quantify to a certain extent the coherence between the modes. The coherence should be further tested by SWIFT,⁴ Intermode Beatnote Spectroscopy,³ dual comb,²⁷ or any suitable coherence measurement.²⁸ Most of these techniques require fast detectors, but a much simpler approach is based on self-mixing, where the QCL itself acts as a fast heterodyne detector.¹⁰ The self-mixing technique can verify to some extent the coherence of the modes in addition to electrical beatnote detection and IFG symmetry consideration and was first presented in Ref. 29 for single plasmon waveguide THz lasers.

The self-mixing coherence setup is sketched in [Fig. 3\(a\)](#) where a 4 mm long and 64 μm wide QCL is aligned to an FTIR and the electrical beatnote is detected over the bias-line. It is important to notice that double-metal THz devices are intrinsically less sensitive to feedback as compared to mid-IR lasers, due to the high impedance mismatch of the double-metal waveguide that provides a high facet reflectivity. This allows the use of self-mixing techniques that are not destroying the comb state as it is observed in the mid-IR.¹³ The FTIR operates in step scan where for each step, the beatnote intensity and frequency are recorded. From the single mode self-mixing theory of Lang-Kobayashi,³⁰ a weak feedback of the optical mode itself will lead to a slight frequency shift of the optical mode frequency. In the experiment, the feedback comes from the FTIR that filters the optical modes as well. In the case of a frequency comb, each mode experiences a feedback at its own frequency which will lead to its shift. Since all modes are locked coherently, the shift induced to one mode will influence all other modes and their spacing, and therefore, the beatnote frequency

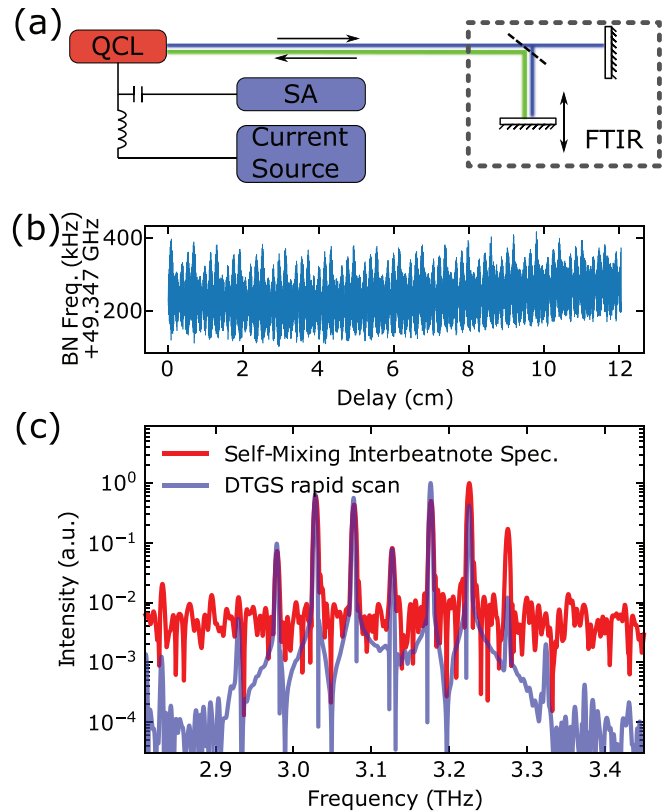


FIG. 3. Self-mixing intermode beatnote (SMIB) spectroscopy experiment. (a) sketches the setup where the FTIR provides a slight feedback as a function of delay and the induced beatnote frequency shift is recorded by the SA. (b) shows the uncorrected SMIB IFG. The slow drift arises from temperature drifts. (c) compares the SMIB spectrum with the FTIR spectrum showing the coherence of the modes.

has to be adjusted slightly. This allows us to measure the effect of self-mixing by the frequency change of the beatnote of a laser in a comb state. A more rigorous mathematical discussion and experimental data of this concept were first presented in Ref. 29. We already applied this self-mixing intermode beatnote (SMIB) spectroscopy technique on a single double-metal (Au–Au) THz waveguide emitting simultaneously two unlocked combs spaced by an octave with two independent beatnotes.³¹ We showed that the detected self-mixing signal is sensitive to its generating comb but not to the other, indicating that indeed only coherent modes determine the beatnote shift, whereas incoherent do not. This approach is applied to the harmonic state presented in [Fig. 1](#), the uncorrected SMIB IFG is shown in [Fig. 3\(b\)](#), and the SMIB spectrum is shown in [Fig. 3\(c\)](#). The induced beatnote change is on the order of 10^{-6} of its frequency, and the slow drift arises from slight temperature changes. By comparing the SMIB spectrum with the DC FTIR intensity spectrum, we see that all observed modes are coherently locked and produce the beating signal, showing the coherent harmonic comb state. It has to be noted that the SMIB cannot fully verify the degree of coherence as it does not provide any information about the relative phases of the modes.

Furthermore, RF injection locking is widely used for comb repetition rate stabilization.^{22,32,33} In the following, we show that a THz harmonic comb displaying a strong free running narrow beatnote, as shown in Fig. 4(a), can be injection locked as well. The RF signal is set to a frequency of roughly 600 kHz away from the beatnote. While increasing the injection power from -18 dBm at the synthesizer output up to 5 dBm typical pulling (red dashed line), the appearance of sidemodes (purple dashed lines) and final locking at 2 dBm are observed as presented in Fig. 4(b). The locking range at 2 dBm is roughly 1.2 MHz.

Besides the experimental findings of harmonic combs in THz QCLs and their stabilization and coherence measurement, we develop a theoretical model supporting their formation and appearance. We argue that the harmonic comb regime in our lasers is facilitated by the asymmetric gain shape created by the interplay of two optical transitions with comparable but different magnitudes of the dipole moment. This is in fact a common feature of THz QCLs with a diagonal transition design. To be specific, here, we use an active region model that includes one common upper laser state and two lower laser states (see Fig. S1 of the supplementary material). Following the approach similar to the one in Ref. 34, we calculate the gain, amplitudes, and phases of weak sidebands generated in the presence of a single strong lasing mode. The details of the calculations and the numerical parameters

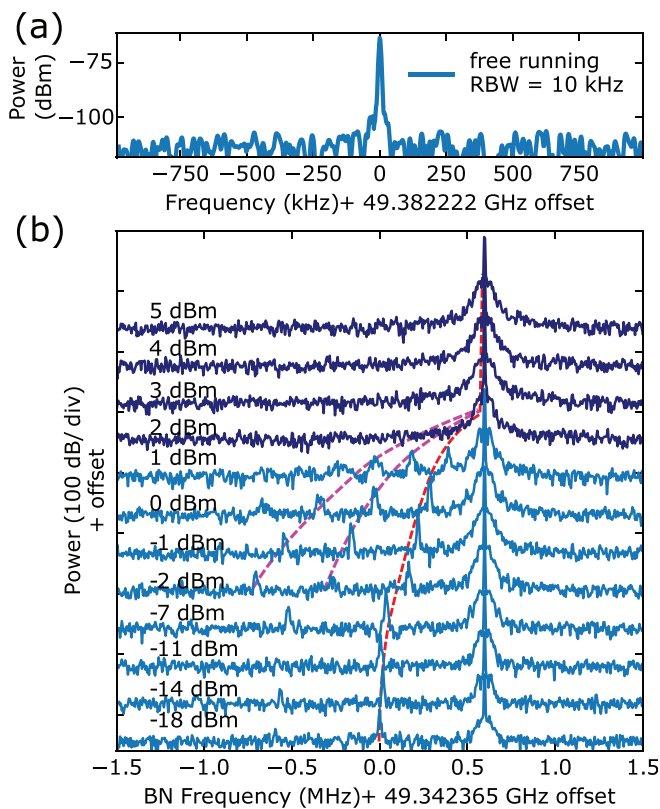


FIG. 4. (a) Presents a free-running beatnote for the laser operating on the fifth harmonic state. (b) shows the beatnote injection locking as a function of increasing RF power (from the bottom). Typical sidebands are visible, and dashed lines are given as guides to the eye.

are described in the Supplement. The formalism is based on the density-matrix equations coupled to the wave equation for the EM field. Since the frequencies of the optical transitions are close to each other, around 10 and 13 meV according to band structure calculations, both of them contribute to the optical polarization and laser field. First, we find the field of a strong laser mode in the third-order nonlinear approximation; then, we calculate the gain and eigenstates of weak side modes. At least two side modes have to be included as they are coupled through a strong central mode in the four-wave mixing process.

Figure 5 presents the net gain, the amplitudes, and the phases of weak side modes E_{s+} , E_{s-} for three different cases: (i) only one optical transition with the dipole moment of 3.7 nm, (ii) two symmetric optical transitions with equal dipole moments equal to 2.6 nm each, and (iii) two asymmetric optical transitions with dipole moments equal to 3.0 nm and 2.1 nm. The dipole matrix elements in the first two cases are chosen so that the values of $d_{ul_x}^2 + d_{ul_p}^2$ are unchanged from the third case, and hence, the total gain coefficients in all cases are similar. From Comsol simulations of the waveguide modes, we took the total cavity decay rate corresponding to the field propagation loss of 6.5 cm^{-1} and the group velocity dispersion (GVD) of $6.35 \times 10^4 \text{ fs}^2/\text{mm}$. Comparing the gain spectra in Fig. 5(a), one can see that for a single optical transition or two symmetric optical transitions, the net gain of weak side modes is positive starting from zero detuning, which indicates that multimode lasing can start from adjacent modes favoring the dense laser spectrum. Only in the case of two asymmetric optical transitions, the net gain of side modes is negative at small frequency detunings, preventing lasing on adjacent modes and favoring the harmonic state. As we show in Fig. S4 of the supplementary material in more detail, there is an optimal range of asymmetry ratios $d_{ul_x}^2 / (d_{ul_x}^2 + d_{ul_p}^2)$, which maximizes the magnitude of the negative gain.

Figure 5(b) shows that the net gain of the weak side modes for two asymmetric optical transitions increases with the pumping level and its peaks move to larger frequency detunings. The suppression of gain around zero frequency detuning gets stronger with increasing pumping and reaches its maximum and then starts decreasing again as the pumping continues to increase. This indicates that the harmonic state is favored within a specific range of pumping levels.

Figure 5(c) shows that in the case of two asymmetric optical transitions, the phase difference between the two side modes is around π . However, the amplitudes are very different, which indicates that the laser field is not FM, and it will have strong amplitude modulation. As we discuss in Ref. 34 in more detail, the AM component in the optical field makes negative contribution to the sideband gain. It lowers the net gain to negative values at small detunings, suppressing the proliferation of neighboring modes and favoring the harmonic state. This provides a qualitative physical explanation why the presence of two asymmetric optical transitions can support the self-starting harmonic comb. In contrast, in the case of one optical transition and two symmetric optical transitions, the two weak side modes have similar amplitudes at small frequency detunings (<30 GHz), and their phase relations indicate the FM field. At larger frequency detunings (>50 GHz), the two side modes have different intensities, which is due to the effect of GVD. See the supplementary material for the details on these two cases.

Although not directly relevant to THz QCLs in this study, we also looked at the effect of gain recovery time T_1 on the sideband

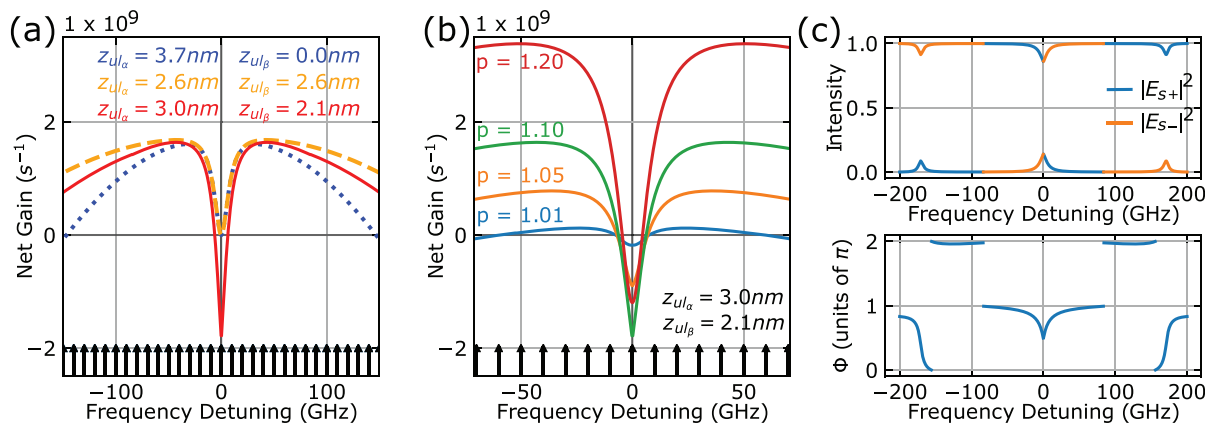


FIG. 5. The instability of weak side modes and their intensities and phases in the presence of a central strong lasing mode as a function of frequency detuning from the central mode for the active region. (a) The net gain at the pumping level of $p = 1.10$ for single optical transition with a dipole moment of 3.7 nm (blue dotted line), two optical transitions with equal dipole moments equal to 2.6 nm (orange dashed line), and two optical transitions with dipole moments equal to 3.0 and 2.1 nm (red line). Fabry-Pérot modes are indicated at the bottom with black arrows for a 4 mm long device. (b) The net gain for two optical transitions with dipole moments equal to 3.0 and 2.1 nm, at pumping levels of $p = 1.01, 1.05, 1.10,$ and 1.20 . Maxima are shifting to higher detunings with higher pumping rates, and net losses around zero detuning decrease after the 1.10 pumping level. Fabry-Pérot modes are indicated at the bottom with black arrows for a 4 mm long device. (c) The intensities and phase difference of the weak side modes at the pumping level of $p = 1.10$. The gain relaxation times are $T_1 = 20$ ps and $T_2 = 0.2$ ps, and the population grating diffusion factor is $D = 100$ cm²/s. Horizontal lines in (a) and (b) indicate zero net gain.

generation. As illustrated in Fig. S2 of the [supplementary material](#), the main effect is that the separation between the peaks in the sideband gain increases with decreasing T_1 . This is expected as the system with a faster T_1 can support a faster dynamics. The width of the negative gain region also increases, whereas the magnitude of the negative dip at zero detuning remains largely the same. This may have interesting implications for the design of mid-IR QCL active regions: the asymmetry in the gain transition introduced by design may help supporting a self-starting harmonic comb.

The results of the linear analysis of the multimode generation for two asymmetric optical transitions are qualitatively consistent with the harmonic lasing state with asymmetric sidebands observed in the experiment. The limitations of weak-side mode approximation prevent us from making any quantitative predictions. The actual multimode lasing state will be determined by the nonlinear competition of many strong laser modes. Its modeling requires fully nonlinear space-time domain simulations, which is beyond the scope of this paper. Still, the presented analysis allows us to follow how the asymmetric harmonic state emerges from the coherent interplay of two optical transitions, which could be a physical mechanism behind the self-starting harmonic comb emission in THz QCLs. Obviously, more studies are needed before a complete physical picture is revealed. It is fascinating, however, how QCLs continue bringing new surprising features to such a well-studied field as fundamental laser dynamics.

In conclusion, we presented multiple THz QCLs operating on self-starting pure harmonic comb states. The electrical narrow and single beatnotes indicate the coherence and can be RF injection locked to an external RF synthesizer. The coherence is further assessed by the SMIB spectrum, showing the coherence of the observed modes. The theoretical model, extended to including two unbalanced optical transitions in our AR design, supports qualitatively our observations of pure harmonic combs in THz QCLs.

See the [supplementary material](#) for the theoretical model for a single optical transition described in Ref. 34 extended to two optical transitions. The theoretical results compare the weak side modes from a single mode instability arising from the asymmetric gain profile with two optical transitions with different dipole moments to the symmetric gain profile with one transition and symmetric gain profile and two transitions with equal dipole moments. Additionally, the light-current-voltage curve for the device shown in Fig. 1 is presented, and we elaborate on the interferogram envelope symmetry argument for pure comb verification by providing numerical simulation of the observed fundamental and harmonic combs in Figs. 1(b) and 1(d) with unequally spaced modes.

We acknowledge the financial support from the H2020 European Research Council Consolidator Grant (No. 724344) (CHIC) and from Schweizerischer Nationalfonds zur Förderung der Wissenschaftlichen Forschung (No. 200020-165639). Y.W. and A.B. acknowledge the support from NSF Grant No. 1807336. We thank the group of U. Keller for lending the 50 GHz signal generator and Martin Franckić for discussions.

DATA AVAILABILITY

The data that support the findings of this study are available from the corresponding author upon reasonable request.

REFERENCES

- ¹J. Faist, F. Capasso, D. L. Sivco, C. Sirtori, A. L. Hutchinson, and A. Y. Cho, "Quantum cascade laser," *Science* **264**, 553–556 (1994).
- ²R. Köhler, A. Tredicucci, F. Beltram, H. E. Beere, E. H. Linfield, A. G. Davies, D. A. Ritchie, R. C. Iotti, and F. Rossi, "Terahertz semiconductor-heterostructure laser," *Nature* **417**, 156–159 (2002).
- ³A. Hugi, G. Villares, S. Blaser, H. C. Liu, and J. Faist, "Mid-infrared frequency comb based on a quantum cascade laser," *Nature* **492**, 229–233 (2012).

- ⁴D. Burghoff, T.-Y. Kao, N. Han, C. W. I. Chan, X. Cai, Y. Yang, D. J. Hayton, J.-R. Gao, J. L. Reno, and Q. Hu, "Terahertz laser frequency combs," *Nat. Photonics* **8**, 462–467 (2014).
- ⁵M. Rösch, G. Scalari, M. Beck, and J. Faist, "Octave-spanning semiconductor laser," *Nat. Photonics* **9**, 42–47 (2015).
- ⁶Q. Lu, F. Wang, D. Wu, S. Slivken, and M. Razeghi, "Room temperature terahertz semiconductor frequency comb," *Nat. Commun.* **10**, 2403 (2019).
- ⁷M. Singleton, P. Jouy, M. Beck, and J. Faist, "Evidence of linear chirp in mid-infrared quantum cascade lasers," *Optica* **5**, 948–953 (2018).
- ⁸C. Y. Wang, L. Kuznetsova, V. M. Gkortsas, L. Diehl, F. X. Kärtner, M. A. Belkin, A. Belyanin, X. Li, D. Ham, H. Schneider, P. Grant, C. Y. Song, S. Haffouz, Z. R. Wasilewski, H. C. Liu, and F. Capasso, "Mode-locked pulses from mid-infrared quantum cascade lasers," *Opt. Express* **17**, 12929–12943 (2009).
- ⁹S. Barbieri, P. Gellie, G. Santarelli, L. Ding, W. Maineult, C. Sirtori, R. Colombelli, H. Beere, and D. Ritchie, "Phase-locking of a 2.7-THz quantum cascade laser to a mode-locked erbium-doped fibre laser," *Nat. Photonics* **4**, 636–640 (2010).
- ¹⁰M. Rösch, G. Scalari, G. Villares, L. Bosco, M. Beck, and J. Faist, "On-chip, self-detected terahertz dual-comb source," *Appl. Phys. Lett.* **108**, 171104 (2016).
- ¹¹F. P. Mezzapesa, V. Pistore, K. Garrasi, L. Li, A. G. Davies, E. H. Linfield, S. Dhillon, and M. S. Vitiello, "Tunable and compact dispersion compensation of broadband THz quantum cascade laser frequency combs," *Opt. Express* **27**, 20231–20240 (2019).
- ¹²T. S. Mansuripur, C. Vernet, P. Chevalier, G. Aoust, B. Schwarz, F. Xie, C. Caneau, K. Lascola, C.-E. Zah, D. P. Caffey, T. Day, L. J. Missaggia, M. K. Connors, C. A. Wang, A. Belyanin, and F. Capasso, "Single-mode instability in standing-wave lasers: The quantum cascade laser as a self-pumped parametric oscillator," *Phys. Rev. A* **94**, 063807 (2016).
- ¹³M. Piccardo, P. Chevalier, T. S. Mansuripur, D. Kazakov, Y. Wang, N. A. Rubin, L. Meadowcroft, A. Belyanin, and F. Capasso, "The harmonic state of quantum cascade lasers: Origin, control, and prospective applications [Invited]," *Opt. Express* **26**, 9464–9483 (2018).
- ¹⁴D. Kazakov, M. Piccardo, Y. Wang, P. Chevalier, T. S. Mansuripur, F. Xie, C.-E. Zah, K. Lascola, A. Belyanin, and F. Capasso, "Self-starting harmonic frequency comb generation in a quantum cascade laser," *Nat. Photonics* **11**, 789 (2017).
- ¹⁵F. Wang, V. Pistore, M. Riesch, H. Nong, P.-B. Vigneron, R. Colombelli, O. Parillaud, J. Mangeney, J. Tignon, C. Jirauschek, and S. S. Dhillon, "Ultrafast response of harmonic modelocked THz lasers," *Light: Sci. Appl.* **9**, 51 (2020).
- ¹⁶H. Li, P. Laffaille, D. Gacemi, M. Apfel, C. Sirtori, J. Leonardon, G. Santarelli, M. Rösch, G. Scalari, M. Beck, J. Faist, W. Hänsel, R. Holzwarth, and S. Barbieri, "Dynamics of ultra-broadband terahertz quantum cascade lasers for comb operation," *Opt. Express* **23**, 33270–33294 (2015).
- ¹⁷M. Piccardo, P. Chevalier, S. Anand, Y. Wang, D. Kazakov, E. A. Mejia, F. Xie, K. Lascola, A. Belyanin, and F. Capasso, "Widely tunable harmonic frequency comb in a quantum cascade laser," *Appl. Phys. Lett.* **113**, 031104 (2018).
- ¹⁸D. Kazakov, M. Piccardo, M. Beiser, N. Opacak, Y. Wang, A. Belyanin, B. Schwarz, B. Schwarz, and F. Capasso, "Shaping harmonic frequency combs in ring injection lasers by defect engineering," in *Conference on Lasers and Electro-Optics* (Optical Society of America, 2020), p. STh3E.8.
- ¹⁹D. R. Bacon, J. R. Freeman, R. A. Mohandas, L. Li, E. H. Linfield, A. G. Davies, and P. Dean, "Gain recovery time in a terahertz quantum cascade laser," *Appl. Phys. Lett.* **108**, 081104 (2016).
- ²⁰R. P. Green, A. Tredicucci, N. Q. Vinh, B. Murdin, C. Pidgeon, H. E. Beere, and D. A. Ritchie, "Gain recovery dynamics of a terahertz quantum cascade laser," *Phys. Rev. B* **80**, 075303 (2009).
- ²¹C. G. Derntl, G. Scalari, D. Bachmann, M. Beck, J. Faist, K. Unterrainer, and J. Darmo, "Gain dynamics in a heterogeneous terahertz quantum cascade laser," *Appl. Phys. Lett.* **113**, 181102 (2018).
- ²²A. Forrer, M. Franckić, D. Stark, T. Olariu, M. Beck, J. Faist, and G. Scalari, "Photon-driven broadband emission and frequency comb RF injection locking in THz quantum cascade lasers," *ACS Photonics* **7**, 784–791 (2020).
- ²³A. Forrer, L. Bosco, M. Beck, J. Faist, and G. Scalari, "RF injection of THz QCL combs at 80 K emitting over 700 GHz spectral bandwidth," *Photonics* **7**, 9 (2020).
- ²⁴D. Bachmann, M. Rösch, M. J. Süess, M. Beck, K. Unterrainer, J. Darmo, J. Faist, and G. Scalari, "Short pulse generation and mode control of broadband terahertz quantum cascade lasers," *Optica* **3**, 1087–1094 (2016).
- ²⁵L. Mertz, "Auxiliary computation for Fourier spectrometry," *Infrared Phys.* **7**, 17–23 (1967).
- ²⁶M. L. Forman, W. H. Steel, and G. A. Vanasse, "Correction of asymmetric interferograms obtained in Fourier spectroscopy," *J. Opt. Soc. Am.* **56**, 59–63 (1966).
- ²⁷S. Barbieri, M. Ravaro, P. Gellie, G. Santarelli, C. Manquest, C. Sirtori, S. P. Khanna, E. H. Linfield, and A. G. Davies, "Coherent sampling of active mode-locked terahertz quantum cascade lasers and frequency synthesis," *Nat. Photonics* **5**, 306–313 (2011).
- ²⁸F. Cappelli, L. Consolino, G. Campo, I. Galli, D. Mazzotti, A. Campa, M. S. de Cumis, P. C. Pastor, R. Eramo, M. Rosch, M. Beck, G. Scalari, J. Faist, P. D. Natale, and S. Bartalini, "Retrieval of phase relation and emission profile of quantum cascade laser frequency combs," *Nat. Photonics* **13**, 562 (2019).
- ²⁹M. Wienold, B. Röben, L. Schrottke, and H. T. Grahn, "Evidence for frequency comb emission from a Fabry-Pérot terahertz quantum-cascade laser," *Opt. Express* **22**, 30410–30424 (2014).
- ³⁰R. Lang and K. Kobayashi, "External optical feedback effects on semiconductor injection laser properties," *IEEE J. Quantum Electron.* **16**, 347–355 (1980).
- ³¹A. Forrer, M. Rösch, M. Singleton, M. Beck, J. Faist, and G. Scalari, "Coexisting frequency combs spaced by an octave in a monolithic quantum cascade laser," *Opt. Express* **26**, 23167 (2018).
- ³²P. Gellie, S. Barbieri, J.-F. Lampin, P. Filloux, C. Manquest, C. Sirtori, I. Sagnes, S. P. Khanna, E. H. Linfield, A. G. Davies, H. Beere, and D. Ritchie, "Injection-locking of terahertz quantum cascade lasers up to 35GHz using RF amplitude modulation," *Opt. Express* **18**, 20799–20816 (2010).
- ³³J. Hillbrand, A. M. Andrews, H. Detz, G. Strasser, and B. Schwarz, "Coherent injection locking of quantum cascade laser frequency combs," *Nat. Photonics* **13**, 101–104 (2019).
- ³⁴Y. Wang and A. Belyanin, "Harmonic frequency combs in quantum cascade lasers: Time-domain and frequency-domain theory," *Phys. Rev. A* **102**, 013519 (2020).